tvst

Article

Intrinsic Optical Properties of Boston Keratoprosthesis

Pui-Chuen Hui[1,2], Leonardo A. Pereira[1,3], Renald Dore[4], Shengtong Chen[4], Elise Taniguchi[1,2], James Chodosh[1], Claes H. Dohlman[1,2], and Eleftherios I. Paschalis[1,2]

[1] Department of Ophthalmology, Massachusetts Eye and Ear, Harvard Medical School, Boston, MA, USA
[2] Schepens Eye Research Institute, Boston Keratoprosthesis Laboratory, Massachusetts Eye and Ear, Harvard Medical School, Boston, MA, USA
[3] CAPES Foundation, Ministry of Education of Brazil, Brasilia, Brazil
[4] University of Rochester, Institute of Optics, Rochester, NY, USA

Correspondence: Eleftherios I. Paschalis, Department of Ophthalmology, Boston Keratoprosthesis Laboratory, Massachusetts Eye and Ear and Schepens Eye Research Institute, Harvard Medical School, Boston, MA 02114, USA. e-mail: eleftherios_paschalis@meei.harvard.edu

Received: May 29, 2020
Accepted: September 7, 2020
Published: November 3, 2020

Keywords: Boston Keratoprosthesis; optics; artificial cornea

Citation: Hui P-C, Pereira LA, Dore R, Chen S, Taniguchi E, Chodosh J, Dohlman CH, Paschalis EI. Intrinsic optical properties of Boston Keratoprosthesis. Trans Vis Sci Tech. 2020;9(12):10, https://doi.org/10.1167/tvst.9.12.10

Purpose: To benchmark the optical performance of Boston Keratoprosthesis (B-KPro).

Methods: Back focal lengths (BFL) of B-KPros for various eye axial lengths were measured using an optical bench, International Organization for Standardization–certified for intraocular lens characterization, and compared against manufacturer's specification. The modulation transfer function (MTF) and the resolution efficiencies were measured. The theoretical geometry-dependent higher-order aberrations (HOA) were calculated. The devices were characterized with optical profilometry for estimating the surface scattering. Aberration correction and subsequent image quality improvement were simulated in CODE-V. Natural scene-imaging was performed in a mock ocular environment. Retrospective analysis of 15 B-KPro recipient eyes were presented to evaluate the possibility of achieving 20/20 best-corrected visual acuity (BCVA).

Results: BFL measurements were in excellent agreement with the manufacturer-reported values ($r = 0.999$). The MTF specification exceeded what is required for achieving 20/20 visual acuity. Astigmatism and field curvature, correctable in simulations, were the primary aberrations limiting imaging performance. Profilometry of the anterior surface revealed nanoscale roughness (root-mean-square amplitude, 30–50 nm), contributing negligibly to optical scattering. Images of natural scenes obtained with a simulated B-KPro eye demonstrated good central vision, with 10/10 visual acuity (equivalent to 20/20). Full restoration of 20/20 BCVA was obtainable for over 9 years in some patients.

Conclusions: Theoretical and experimental considerations demonstrate that B-KPro has the optical capacity to restore 20/20 BCVA in patients. Further image quality improvement can be anticipated through correction of HOAs.

Translational Relevance: We establish an objective benchmark to characterize the optics of the B-KPro and other keratoprosthesis and propose design changes to allow improved vision in B-KPro patients.

Introduction

The Boston Keratoprosthesis (B-KPro) artificial cornea has been recognized as an effective alternative treatment for patients with intractable corneal blindness not amenable to standard penetrating keratoplasty.[1,2] Two types of B-KPro devices are clinically available: types I and II. The type II device is primarily used in selected cases with severe ocular surface diseases, such as Steven Johnson's syndrome and mucous membrane pemphigoid.[3] However, the type I B-KPro is the most commonly and successfully used keratoprosthesis around the world, with over 15,000 devices implanted thus far, providing an ideal alternative for patients not amenable to standard corneal transplantation but with an otherwise healthy ocular surface.[4] Both types are made of a medical-grade polymethylmethacrylate (PMMA) optical stem/front plate, and a back plate made of either PMMA or

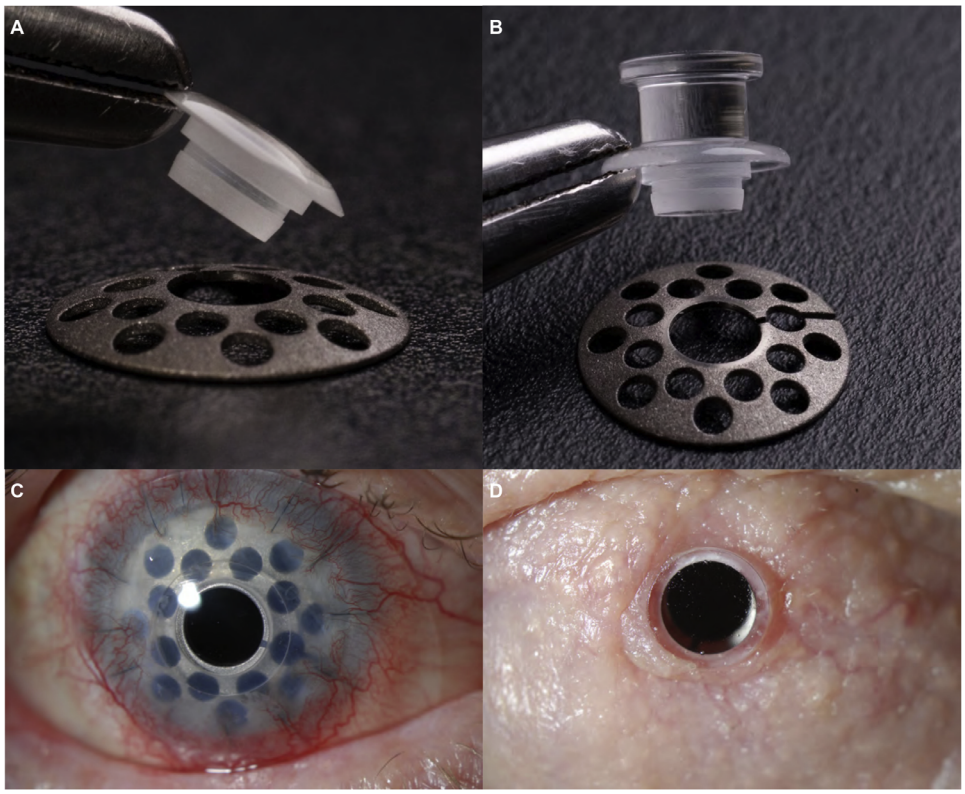

Figure 1. B-KPro types I and II before and after implantation in the eye. (A) B-KPro type I, which has an optical stem and front plate made of PMMA, and a back plate made of either PMMA or as shown, of titanium. The holes in the back plate allow aqueous humor diffusion to the donor cornea. Diameter of the optical stem is 3 mm. (B) B-KPro type II has an extra anterior cylinder, which protrudes through an opening in the eyelid skin. (C) Implanted B-KPro type I. A corneal graft is used as a carrier between the front and back plates, and the device-graft combination is sutured to the eye in the same fashion as a penetrating keratoplasty. (D) Implanted B-KPro type II. Note the extra anterior cylinder protruding through the closed lid that has undergone permanent medial and lateral tarsorrhaphy.

titanium.[5,6] A corneal graft is required as carrier tissue for the device, and is sutured to the eye in the same fashion as a penetrating graft. Subsequently, the type I B-KPro recipient eye is usually fitted with a soft contact lens. The type II B-KPro has an extra anterior cylinder, which protrudes through an opening in surgically closed eyelids and does not require or permit fitting of a soft contact lens (Figs. 1A–D).[7]

The surgical and clinical outcomes of patients implanted with the B-KPro have been previously published to elucidate the clinical performance of the device,[8,9] and help surgeons optimize patient selection and reduce postoperative surgical complications. A few studies have detailed the optical performance of the B-KPro,[10–12] however, a detailed evaluation of the intrinsic optical performance of the B-KPro simulating an aqueous environment has not been performed to International Organization for Standardization (ISO) standard bench-top methods. We have addressed this gap by adopting the ISO standards for implantable intraocular lenses (IOLs) for benchmarking the optical properties of the B-KPro type I device, which is the most frequently implanted B-KPro type. In particular, the back focal length (BFL), modulation transfer function (MTF), and the resolution efficiency were measured for B-KPro devices of various focal lengths. Moreover, as in the cases of refractive surgeries, higher-order aberration (HOA) calculations are necessary to assess the entire optical performance of the device and its ability to project a clear image to the retina. Hence using the Seidel aberration framework, we evaluated the theoretical wavefront aberration according to the geometry of the B-KPro optical component. Also, we performed surface profilometry to evaluate the surface irregularities that scatter light and determined the extent of scattering over the imaging performance. We complemented this battery of characterizations with a demonstration of natural scene-imaging with a B-KPro in a mock ocular environment. Finally, we provided clinical data from patients implanted with the device

to demonstrate B-KPro's ability to achieve 20/20 vision and discuss future modifications that could enhance the quality of vision experienced by B-KPro recipients.

Methods and Materials

BFL Measurement and Verification of the Dioptric Power Recommendation for Different Eye Axial Lengths

All B-KPro devices used in this study adhered to the ISO 11979-2:2014 optical quality standard, as regulated by the US Food and Drug Administration for class II devices. The BFL of 15 different dioptric power B-KPro devices were measured using the Optikos (Wakefield, MA) bench equipped with a charge-coupled device (CCD), a bandpass filter centered at $\lambda = 546$ nm and 3 mm aperture, operated under ISO 11979-2:1999 standards.[13] The agreement between the manufacturer-specified BFLs and the Optikos BFL measurements were compared and statistically analyzed using Pearson's correlation coefficient, Lin's concordance correlation coefficient (CCC), and bias correlation factor (C_b). A linear line was also fitted to these two parameters and the presence of a zero offset was statistically tested.

To verify the empirically determined B-KPro dioptric power recommendation for aphakic eyes of different axial lengths, we considered a model where the sum of the axial length of the eye and the protrusion of the B-KPro from the cornea's apex (which we termed the "postoperative axial length") should be equal to the thickness of the B-KPro lens plus the BFL in aqueous/vitreous humor. Here the BFL in aqueous/vitreous humor is simply given by the measured BFL in air multiplied by the refractive index of the humor (i.e., 1.337). The protrusion of the B-KPro from the apex of the cornea can be calculated from simple geometry using the B-KPro's radius of curvature, the preoperative axial length of the eye, and the diameter of the B-KPro's front plate. We plot the sum of the B-KPro lens thickness (i.e., 2.89 mm) and the BFL in the humor against the recommended axial length of the eye. The absolute difference between the sum concerned and the postoperative axial length is also plotted to assess any underlying sources of potential deviation. Moreover, we compare this difference against the theoretical depth of focus of each lens (given by $\frac{4.88\lambda f^2}{D^2}$ where λ is the wavelength chosen at 550 nm, D is the B-KPro aperture of 3 mm, and f is the focal length of the B-KPro) to assess how well the depth of focus could accommodate such deviation.

Imaging Quality and MTF Measurements

The imaging quality of B-KPro devices and the MTF were determined for the 15 B-KPro lenses using the Optikos bench in air. The optical setup was constructed based on the Annex B and C of ISO11979-2 *Ophthalmic implants — Intraocular lenses — Part 2: Optical properties and test methods*.[13] To obtain the resolution efficiency, the USAF 1951 Resolution Target was imaged with a telescope (magnification of ~10) consisting of a fixed collimator and the B-KPro device being tested. The finest resolved group of elements was then determined. The corresponding spatial frequency of the resolved patterns was compared against the diffraction-limited cut-off spatial frequency of a perfect lens possessing the identical focal length of the B-KPro device. Specifically, the resolution efficiency (RE) is given by $RE = 2^{[G+(E-1)/6]} \times \frac{\lambda F}{D}$, where G and E are the group and the element within of the finest resolved pattern respectively, F is the telescope's collimator effective focal length (set as 181 mm), λ is the test wavelength (set as 546 nm), and D is the test aperture diameter (set as 3 mm). To obtain the MTF, a pinhole (instead of the resolution target) was imaged by the same setup. Fourier transform of the resultant line spread function gives the MTF of the device under test. The MTF was reported in both the tangential and sagittal directions of the optics.

HOA Calculation

In the thin lens limit, the optical aberrations of the B-KPro were reported using the wavefront/optical path length aberration measures. The Seidel HOA of the B-KPro was evaluated based on the five major third-order Seidel aberrations, that is (on-axis) spherical aberration (A_{SA}), (off-axis) astigmatism, field curvature, coma and distortion were calculated using paraxial parameters of the B-KPro.[14] A_{SA} is evaluated using $A_{SA} = -\frac{1}{32n(n-1)f^3}[\frac{n^3}{n-1} + (3n+2)(n-1)p^2 + \frac{n+2}{n-1}q^2 + 4(n+1)pq](\frac{D}{2})^4 = a_s(\frac{D}{2})^4$, where D is the diameter of the B-KPro aperture. Because the B-KPro is a convex-plano lens, the shape factor q is set as +1 while the position factor/ conjugate ratio p is set as –1 for an object placed at infinity. The peak amplitude of coma is given by $A_c = \frac{h'(\frac{D}{2})^3}{4nf^2S'}[(2n+1)p + \frac{n+1}{n-1}q] = a_c h'(\frac{D}{2})^3$, where h' is image height and S' is the image position. Replacing the ratio h'/S' with the field angle φ in the paraxial limit, we can also express the peak coma amplitude as $A_c = \frac{(\frac{D}{2})^3\varphi}{4nf^2}[(2n+1)p + \frac{n+1}{n-1}q]$. The astigmatism A_a and the field curvature A_f do not depend on the position and shape factors p and q, and are

expressed as $A_a = -\frac{h'^2}{2fS'^2}(\frac{D}{2})^2 = a_a h'^2(\frac{D}{2})^2 = -\frac{\varphi^2}{2f}(\frac{D}{2})^2$ and $A_f = -\frac{(n+1)h'^2}{4nfS'^2}(\frac{D}{2})^2 = a_f h'^2(\frac{D}{2})^2 = -\frac{(n+1)\varphi^2}{4nf}(\frac{D}{2})^2$, respectively. The distortion aberration of a thin lens is zero with the aperture stop coinciding with the lens where the chief ray height is zero. Finally, the total wavefront aberration $W(r, \theta)$ was also plotted as a function of the aperture coordinates (r, θ): $W(r, \theta) = a_s r^4 + a_c h' r^3 \cos(\theta) + a_a h'^2 r^2 \cos^2(\theta) + a_f h'^2 r^2$ to visualize the distribution of aberrations over the entire image field.

In addition, a wide-field two-dimensional (2D) image simulation was performed in CODE V (Synopsys, Inc., Mountain View, CA), an optical system design software, to evaluate the projected image after passing through the B-KPro optics. Aberration correction was also simulated to evaluate the improvement in the image formation.

Surface Roughness and Optical Scattering

The root mean squared (RMS) surface roughness σ was obtained using a white light interferometry-based profilometer (NewView 600; Zygo Corporation, Middlefield, CT). The amount of surface roughness-induced diffuse reflectance of an optical surface relative to the specular reflectance was inferred through its total integrated scattering (TIS), given by the Bennet-Porteus equation[15]: $TIS = R_0(\lambda)[1 - e^{-(\frac{4\pi\sigma\cos\theta_i}{\lambda})^2}]$, depends on the wavelength λ and angle of the incident light θ_i, the surface roughness σ, and the reflectivity of the lens/material R_0.

Imaging Natural Scenes with B-KPro in a Simulated Ocular Environment

To simulate the real-life imaging condition in which the posterior surface of a B-KPro was immersed in an aqueous medium, we constructed an imaging apparatus consisting of a cuvette, relay lenses, and an imager. A leak-proof cuvette with a diaphragm clamping the B-KPro was constructed and filled with distilled water (refractive index, 1.333 in the visible range) to simulate the aqueous humor (refractive index, 1.336). The cuvette length matches the B-KPro's apparent focal length in water. The back side of the cuvette was sealed off by a thin glass cover slip with minimal aberration contribution. The image formed by the B-KPro was relayed to a CCD camera (DMK23GM021, The Imaging Source, Charlotte, NC; sensor dimensions: 4.8 x 3.6 mm) via a pair of achromatic doublets (focal lengths, 50 mm; magnification, 1X) in a 4*f* configuration. Natural scenes and an eye chart were imaged through this imaging system.

Clinical Validation

To provide clinical evidence that the B-KPro optics enable 20/20 vision in living human eyes, a retrospective chart review of B-KPro patients was performed. A database of KPro patients eligible to participate in a prior KPro study[16] was accessed, as approved by the institutional review board at Massachusetts Eye and Ear (MEE), and in accordance with HIPAA regulations and with adherence to the tenets of the Declaration of Helsinki. All patients included underwent B-KPro implantation at MEE. Demographic information is provided in the Table in addition to clinically relevant information of each patient, such as indications for B-KPro surgery, preoperative eye axial lengths, the presence of aphakia or pseudophakia, and the time at which 20/20 vision was attained.

Results

Back Focal Length

BFL measurements in air performed with the Optikos were in excellent agreement with the manufacturer's measurements/specification, Pearson's correlation coefficient r = 0.999, $P < 0.0001$, CCC = 0.999, and $C_b = 0.999$ (Fig. 2A). A linear fit was performed to the data. The slope was fitted to be 1.007 (confidence interval [CI], 0.992, 1.021). The zero offset was fitted to be –0.227 mm (CI, –0.466, 0.011) and its difference from zero was not statistically significant ($P = 0.276$). Figure 2B shows the relationship between the measured dioptric powers and the specified lens curvatures: the measured dioptric powers follow an inverse power law with the lens curvatures, as indicated by the lensmaker equation applied to a convex-plano lens. Finally, we verified the appropriateness of the suggested lens dioptric power for each preoperative axial length. Figure 2C shows a simple model where the sum of the B-KPro's thickness and the BFL in the aqueous humor should equate the postoperative axial length (defined as the sum of the preoperative axial length of the eye and the anticipated protrusion of the B-KPro from the cornea's apex). Figure 2D plots the sum of the B-KPro central optic thickness and the BFL in the eye against the recommended preoperative axial length. Figure 2E shows the absolute deviation of the parameter of the B-KPro thickness + BFL in an eye from the postoperative axial length (blue squares: light blue for positive values in the difference; dark

Table. Demographics and Visual Outcomes of Patients Without Significant Retinal Pathology

#	Age (years)	Sex	Preoperative Eye Axial Length (mm)	Indication for B-KPro Surgery	BCVA After B-KPro Implantation	Presence of IOL
1	62	M	22.57	Graft failure after HSV keratitis	20/20 (at 22-month visit)	Aphakic
2	28	F	Data unavailable	CHED	$20/20^{-1}$ (at 8-year visit)	Pseudophakic
3	64	M	22.21	Chemical burn	20/20 (at 6- to 24-month visit[a])	Pseudophakic
4	48	M	22.34	Trauma	20/20 (within 3 months postoperative)	Pseudophakic
5	44	M	22.48	Explosion injury	20/20 (within 3 months postoperative)	Pseudophakic
6	78	M	25.41	Salzmann's nodular degeneration with scarring	20/20 (at 20-month visit; sustained through 7-year visit)	Aphakic
7	73	F	Data unavailable	Neurotrophic keratopathy	$20/20^{-1}$ (at 6- to 24-month visit[a]; sustained through 6-year visit)	Pseudophakic
8	54	M	23.94	Corneal perforation	$20/20^{-2}$ (at 4-year visit)	Aphakic
9	57	M	28.15	Aniridic keratopathy	20/20 (at 14-month visit)	Pseudophakic
10	69	M	Data unavailable	Postpseudomonas keratitis; multiple graft failures	20/20 (within 3 months postoperative)	Aphakic
11	54	F	24.68	Autoimmune keratitis; limbal stem cell deficiency; graft failures	20/20 (at 6-month visit)	Aphakic
12	73	F	22.7	HSV keratitis; graft failures	20/20 (at 9-year visit)	Aphakic
13	27	F	Data unavailable	Chemical injury; graft failures	20/20 (at 20-month visit)	Aphakic
14	48	M	Data unavailable	Alkali burn; graft failures	20/20 (at 7-month visit)	Aphakic
15	80	M	Data unavailable	Chemical burn	20/20 (at 17-month visit)	Aphakic

Clinical validation of the optical performance of the B-KPro lens was retrospectively performed using charts of 15 type-I B-KPro recipient eyes from 15 patients who were able to achieve postoperative BCVA of 20/20. Patient demographics, indications for B-KPro surgery, and clinical condition after surgery were included. The mean age $\pm$ SD of patients was 57 $\pm$ 16 years; 67% were male (n = 10). The primary indication for B-KPro surgery was previous graft failure. Some 60% of eyes were aphakic (n = 9) and 40% pseudophakic (n = 6).

CHED, corneal hereditary endothelial dystrophy; F, female; HSV, herpes simplex virus; IOL, intraocular lens; M, male.

[a]The exact time at which the patient achieved BCVA 20/20 was not available; a range of time is provided instead.

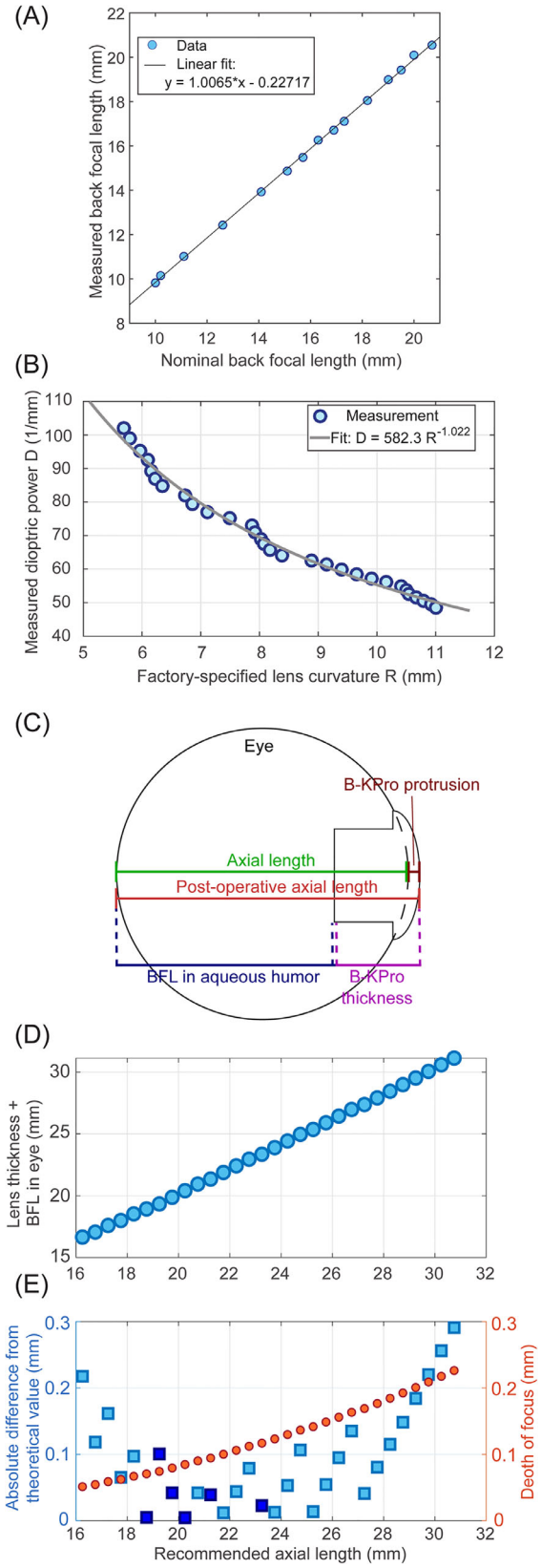

Figure 2. Validation of BFLs and dioptric powers of B-KPro. (A) Comparison of the BFL measurements from the Optikos bench against the factory-specified values. The gray line represents a linear fit where the fitted slope and intercept provide useful pertinent information to validate the agreement statistically. (B) Comparison of the measured dioptric power for each factory-specified lens curvature. The gray line is a fit whose functional form was motivated by the lensmaker equation for a plano-convex lens. (C–E) Validation of the lens recommendation for aphakic eyes of various axial lengths: (C) Schematic representation of the B-KPro eye model where the sum of the B-KPro thickness and the calculated BFL in the aqueous humor is compared with the postoperative eye axial length (defined as the sum of the preoperative eye axial length and the B-KPro protrusion beyond the cornea apex); (D) sum of the B-KPro central optic thickness and the BFL in the eye plotted against the recommended axial length; (E) absolute difference between such sum and the postoperative axial length for each preoperative axial length (*blue squares*: *light blue* for positive value of the actual difference; *dark blue* for negative value of the actual difference). The theoretical depth of focus of each lens (*red circles*) are also plotted.

blue for negative values in the difference). The absolute difference from the postoperative axial length ranged from 0.004 to 0.291 mm. When the differences were normalized by the corresponding recommended axial lengths, the percentage difference ranged from 0.02% to 1.34%. The depth of focus of each lens (red circles) was also plotted to evaluate whether the deviation from the postoperative axial length could be accommodated optically. For a B-KPro whose recommended preoperative axial length exceeds 17.5 mm, the depth of focus is sufficiently large to allow for deviation from the postoperative axial length.

Imaging Quality and MTF

The 1951 USAF resolution test target was imaged with the 15 B-KPro devices. Figure 3A shows the image formed by a B-KPro device with a BFL of 14.9 mm (for eyes with an axial length of 23–23.5 mm). The B-KPro devices were able to resolve elements of 1 to 4 in the group 4 in the resolution target in the telescopic setup. This corresponds to a target resolution frequency of 16 to 22.6 lp/mm at the source. The resolution efficiency of the 15 B-KPro devices was averaged to be 60% (SD, 7%). Figure 3B shows plots of the MTF of four representative B-KPro devices (BFL: 14.86, 16.26, 19.43, and 20.54 mm), both in the tangential direction (blue) and in the sagittal direction (red). The diffraction limit for each device was also plotted (black). The achieved resolution for each B-KPro device was extracted at an MTF value of 0.2 (Fig. 3Ci) and an MTF value of 0.05 (Fig. 3Cii), respectively. (The achieved resolution for devices of BFL <14 mm was not reported for MTF value of 0.05 because the MTF value at the detection limit, i.e., 300 lp/mm, was still >0.05.) The average resolution achieved for the tested B-KPro lenses was 125.6 ± 33.0 (207.2 ± 33.9) lp/mm at an MTF value of 0.2 (0.05). Significant

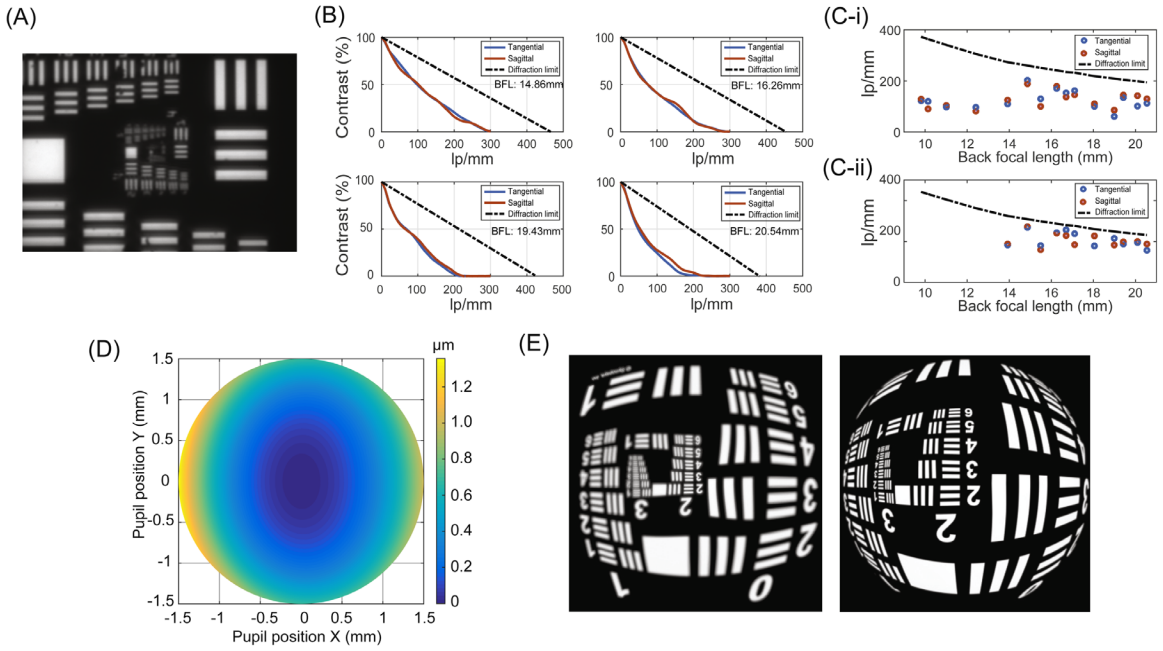

Figure 3. Image quality, MTF measurements, and optical aberrations: (A) 1951 USAF Resolution Test Target imaged in a telescopic configuration (magnification: 10x) using a B-KPro device with a BFL of 14.9 mm. (B) MTF measurements of four representative B-KPro devices (BFL: 14.86, 16.26, 19.43, and 20.54 mm), both in the tangential direction (*blue*) and in the sagittal direction (*red*). The diffraction limit for each device was plotted in black. (C) The achieved resolution (in unit of lp/mm) for each B-KPro device extracted at (i) MTF contrast of 20% and (ii) 5%. (D) Total Seidel third-order wavefront aberration of a B-KPro device modeled as a thin lens. (E) Wide-field CODE V simulation of how an image would form after passing through the B-KPro lens without aberration compensation (*left*) and with the use of lens for aberration compensation (*right*).

differences between tangential and sagittal MTF measurements were only present in two lenses, namely the BFL 12.1 mm lens with tangential resolution approximately 80 lp/mm and sagittal resolution approximately 125 lp/mm at MTF of 0.2, and the BFL 21 mm lens with tangential resolution approximately 60 lp/mm and sagittal resolution approximately 100 lp/mm.

Optical Aberrations

With the shape factor q set as $+1$ while the position factor/conjugate ratio p set as -1 for an object placed at infinity, A_{SA} is simplified as $A_{SA} = -\frac{n^3-2n^2+2}{8n(n-1)^2 f^3}(\frac{D}{2})^4$. For a lens with an effective focal length (EFL) of 17.5 mm, the wavefront aberration due to spherical aberration was 0.286 μm. Similarly, with q set as $+1$ and p set as -1, the coma is given by $A_c = 2.04 \times 10^{-6}\phi$ μm. The peak astigmatism value is given by $A_a = -64.3\phi^2$ μm and the peak field curvature $A_f = -53.7\phi^2$ μm. Assuming a pencil of parallel beams incident on the B-KPro at an angle φ of 5° from the optical axis, the peak wavefront aberration was 0.178 μm due to coma, 0.490 μm due to astigmatism, and 0.409 μm owing to the field curvature. The overall wavefront aberration as a function of the lens aperture position is shown in Figure 3D. The RMS aberration amplitude is 0.275 μm (approximately half of the visible wavelength at 550 nm); the aberration amplitude reaches 1 μm in the periphery, contributed mostly by the astigmatism and field curvature aberrations.

Wide-field 2D CODE V simulations demonstrated that the 1951 USAF target after passing through a 69D simulated B-KPro lens appeared curved and blurred at the edges (Fig. 3E left). Aberration correction with spectacles provided a visually sharper image, as shown in Figure 3E right.

Optical Profilometry and TIS

Profilometry of the B-KPro anterior surface using white light interferometry showed presence of nanoscale topographic roughness, with a pattern of repeated concentric rings (Fig. 4). The RMS surface roughness of six B-KPro samples ranged from 30 to 50 nm, across an area spanning 140 x 105 μm. From the characterized surface roughness, the corresponding TIS strength was estimated as a function of wavelength using the Bennett-Porteus equation. Scattering is strongest in

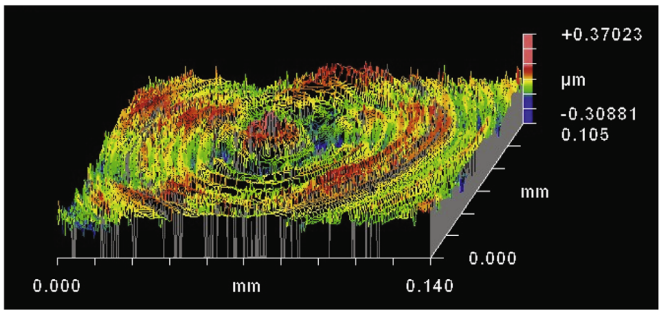

Figure 4. Anterior surface profilometry of the B-KPro: Anterior surface roughness map of a B-KPro lens, measured with surface profilometry. Surface roughness of six B-KPro lenses had a range of RMS amplitude of 30 to 50 nm.

the shorter wavelength range and decreases as the wavelength increases. Also, TIS becomes minimal at large light incident angle. For instance, assuming PMMA reflectance of $R_0(\lambda)\sim4\%$ constant over the visible range (refractive index, 1.495), a B-KPro lens with RMS roughness of 30 nm has a TIS that spans from 1% (at 700 nm) to 2.76% (at 350 nm) at normal incidence, whereas 50-nm roughness generates a TIS that spans from 2.2% (at 700 nm) to 3.84% (at 400 nm).

Images of Natural Scenes through the B-KPro in a Mock Ocular Environment

A schematic of the optical layout and the cuvette built for performing imaging with the B-KPro immersed in an aqueous environment is shown in Figure 5A. The camera sensor accommodates 64% and 48% of the image projected by the B-KPro along the width and the height dimensions, respectively. Images of an outdoor city scene (Fig. 5B) and a Snellen chart placed 10 feet away (Fig. 5C-i) were acquired with the B-KPro (BFL in air, 17.0 mm) mounted in a water-filled cuvette. As seen in the images, the central vision was in focus. By displacing the Snellen chart vertically, we determined the visual angle where the visual acuity dropped below the equivalent 20/20, which was determined to be 3.8° (Fig. 5C-ii). Images of the natural scene in the periphery became gradually defocused and could be refocused by moving the B-KPro toward the imager by approximately 1 mm, that is, the image distance was reduced by 1 mm.

Clinical Correlation

Clinical validation of the optical performance of the B-KPro lens was retrospectively performed using charts of 15 type-I B-KPro recipient eyes from 15 patients who were able to achieve postoperative best-corrected visual acuity (BCVA) of 20/20. The

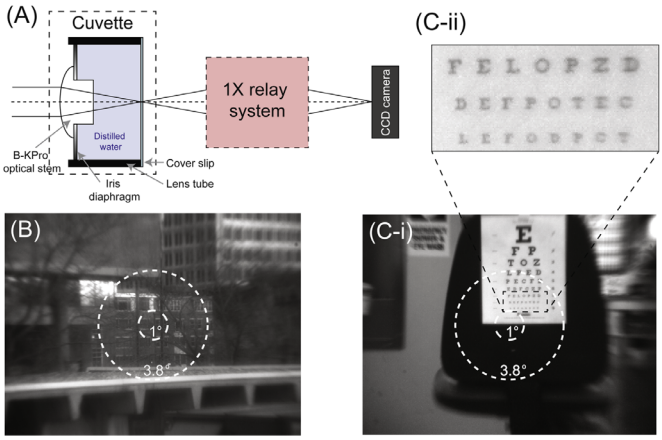

Figure 5. Images of natural scenes through a simulated ocular environment with B-KPro: (A) A labeled schematic of the imaging system for imaging with the B-KPro, consisting of a cuvette for immersing the B-KPro in an aqueous environment, a 1x relay lens system, and an imager (not drawn to scale). (B) An outdoor city scene. (C-i) An eye chart placed 10 feet away from the imaging system. (C-ii) Zoomed-in view of the dotted area on the eye chart encompassing the 20/20-equivalent, 20/25-equivalent, and 20/32-equivalent lines. Letters of the 10/10 line (equivalent to 20/20) could be identified. The area of the optic that confers 20/20 vision corresponds to an equivalent angle of 3.8°.

demographics, the indication for B-KPro surgery, and the visual outcomes of the 15 eyes from 15 patients are shown in the Table. The mean age ± standard deviation (mean ± SD) of patients was 57 ± 16 years; 67% were male (n = 10). A total of 60% of eyes were aphakic (n = 9) and 40% pseudophakic (n = 6). The eye axial lengths ranged from 22.21 to 28.15 mm. Three patients first achieved the BCVA of 20/20 within the first 3 months after the surgery, whereas 9 patients first achieved this within 6 to 24 months postoperation. Of note, 5 patients were able to maintain 20/20 BCVA for 4 to 9 years after the implantation. Despite the variety of corneal diseases leading to B-KPro implantation, those patients with postoperative BCVA of 20/20 illustrated that excellent acuity, when tested under standard conditions, could be achieved with the B-KPro as presently manufactured and implanted.

Discussion

A plethora of studies have been conducted regarding the clinical outcomes of B-KPro surgery, yet very few reports focused on the optical properties of the device and its intrinsic ability to provide normal vision.[10–12,17] There has been confusion as to whether poor visual outcomes in some patients could be attributed to optical limitations of the device. The present study was designed to reevaluate the optics of

the type I B-KPro, validate the manufacturing process and specifications, and determine the optical limits in achieving normal, reasonably glare-free visual acuity. We performed optical characterization of the BFL and the MTF using an optical bench conforming to the ISO standards for IOL characterization and compared the results to the data provided by the manufacturer. We also characterized the surface roughness of the B-KPro and estimated the extent of polishing-induced optical scattering. We also assessed the optical performance of the B-KPro in a simulated ocular environment, thereby providing a realistic representation of the image formed on the retina. Finally, we presented clinical data from a cohort of B-KPro recipients to verify that the B-KPro optics enable the restoration of quality vision in recipients.

BFL measurements in air performed by the manufacturer were in excellent agreement with measurements performed using an ISO-certified optical assessment (Fig. 2A). This demonstrates that dioptric power characterization as currently performed in B-KPro devices is sufficient and up to modern IOL standards. The correspondence between the measured BFL and the manufacturer-specified lens curvature follows the inverse power law as indicated by the lensmaker equation (Fig. 2B). Based on the lensmaker equation and geometric consideration, we derived a simple formula for estimating the appropriate eye axial length given the B-KPro radii of curvature, and compared the sum of the B-KPro thickness and the BFL in the aqueous humor against the postoperative axial length of the eye. For the array of B-KPro lenses of various dioptric powers tested, the sum of the B-KPro thickness and the BFL matches with the postoperative axial length within 0.004 to 0.291 mm. Such difference can be well accommodated by each lens's depth of focus as long as the BFL falls in the range of 11.5 to 19 mm (corresponding to preoperative eye axial length of 18.5–29 mm) (Fig. 2C). We note that the B-KPro dioptric power recommendation for each preoperative axial length was derived empirically from clinical data. It is possible that postoperative remodeling may elongate the eye, which could explain the positive difference of the sum of the BFL and the B-KPro thickness from the presumed postoperative axial lengths. Finally, our simple formula may serve as a helpful guide for future generations of KPro designs where the lens thickness is altered. For instance, the current click-on B-KPro devices has a central thickness of 2.89 mm, as opposed to the version with the locking ring whose central thickness was 3.52 mm. Hence the lens recommendation for different axial lengths could be adjusted accordingly.

With respect to the imaging quality of the B-KPro lens, initial work by Sayegh et al.[11] demonstrated that both the computational and the measured point spread function, and the MTF were consistent with excellent visual acuity results often found with the B-KPro, concluding that the device should be able to provide patients with acceptable visual acuity. In our study, we expanded the direct MTF measurements to an array of B-KPro devices of different dioptric powers following the ISO11979-2 recommendation. Our results indicated an average resolution efficiency of 60%, complying with the suggested recommendation for IOL testing. Furthermore, the average resolution achieved at a contrast of 20% was 126 lp/mm in air. We infer the resolution achieved in an ocular environment would be scaled by the refractive index of the aqueous and vitreous humors ($n = 1.337$) and is estimated to be 94 ± 25 lp/mm. Compared with the native optics of the human eye, which has an MTF of 0.2 at 12 lp/mm for a pupil size of 6 mm and an MTF of 0.2 at 25 lp/mm for a pupil size of 3 mm, the B-KPro's theoretical resolution power exceeds that of a human eye, suggesting that B-KPro's optical performance is more than adequate. Finally, discrepancies between tangential and sagittal MTF were attributed to manufacturing variations but were not deemed to be visually significant.

Although the MTF measurements suggest sufficient optical performance to facilitate good vision in patients, we must also point out inherent optical aberrations in the B-KPro as a simple convex-plano lens, which pose limits to its optical performance. According to the aberration calculations from the Seidel theory, and image quality simulations by CODE V, spherical aberration, astigmatism, and field curvature are the major limiting factors of B-KPro optics that reduce image quality. Low-order aberrations can be successfully corrected using spectacles or a contact lens, as shown in the wide-field CODE V simulations (Fig. 3E); the latter is typically worn in B-KPro recipients. In a study by Sokol et al.,[10] a water-filled mini-camera was used as a model of the aphakic human eye to assess the projected image using different KPro devices (non-B-KPro). Despite the common finding of peripheral blur and distortion in all lenses, these aberrations were deemed to be of minor importance. The small aperture size of the B-KPro, partially blocking the marginal rays, reduces the impact of HOAs on patients' vision.[18] In the future, it would be interesting to perform wavefront aberrometry on B-KPro recipients to compare and contrast against the theoretical aberration limits. Such nonstandard measurements would be facilitated by machines that accommodate variable pupil diameters.[19] As a reference to our estimated RMS wavefront aberration amplitude

of 0.275 μm, a prior report suggests that the mean high-order RMS wavefront error of B-KPro patients (N = 5) was 0.3 ± 0.16 μm as measured by a custom-built aberrometer.[20] A caveat of comparing the clinical value against the theoretical aberration value is that the Seidel theory employed in this work does not account for the immersion of the posterior surface of B-KPro in water. Qualitatively, the aberrations of the B-KPro lens that limit its optical resolving power are expected to be reduced when measured in an aqueous environment instead of air. Hence the actual optical imaging quality in an ocular environment should improve compared with the current results in air. Also, as suggested by the MTF measurements, assessing B-KPro patients' contrast sensitivity should provide another dimension to complement the evaluation of a patient's visual outcome and the B-KPro imaging quality.

Glare is reported to be one of the chief complaints from B-KPro patients.[11,21] It has been experimentally established that the main source of forward-scattering was the influence of the donor cornea via the holes in the B-KPro back plate.[11] For the sake of completeness, we provided quantitative estimates of the extent of optical scattering due to manufacturing-induced surface scattering. The amplitude of the surface roughness in the B-KPro was 30 to 50 nm, which is significantly lower than that of human corneal epithelium (~140 nm) or even hydrogel contact lenses (~323 nm) made of nefilcon A.[22,23] From the Bennett-Porteus model, we estimated 1% to 4% of the incident light was scattered, which is a negligible amount and in concordance with previous experimental findings. The ridge-like surface roughness on the anterior surface of the B-KPro lens appeared as a continuous pattern of concentric rings, a manufacturing outcome owing to the computerized lathe processing of the PMMA (Fig. 5B). Reduction of scattering attributable to surface roughness could be achieved by further smoothing of the anterior surface of the B-KPro. Furthermore, the use of a hydrophilic contact lens in B-KPro patients should minimize the effect of surface roughness. Also, the tear film can fill in small irregularities and surface defects, as previously shown in human corneas.[23] This suggests that the contact lens has a role in B-KPro optics beyond maintaining a healthy cornea, minimizing corneal desiccation, and preventing keratolysis. However, even B-KPro type II devices, which have no overlying tear film or contact lens, can still afford 20/15 vision, suggesting that quality vision is possible with a B-KPro even without a tear film or contact lens.

Integrating the knowledge gleaned from the optical characterization with regard to focusing, MTF, optical aberrations, and scattering, we also illustrate the imaging performance of the B-KPro by acquiring images of natural scenes in which a realistic ocular B-KPro imaging condition was mimicked. A 20/20 visual acuity was attained within the angular field of view of 3.8°. Peripheral vision appeared defocused but could be refocused by shortening the imaging distance. This is consistent with optical elements that possess spherical aberrations, where the marginal rays are focused closer to the lens than the paraxial rays and is correctable through a modification in manufacturing. This is expected to improve the quality of peripheral vision as well. The clinical evaluation of patients with B-KPro, without prior or current history of extra-retinal pathology that spares the fovea, confirmed that the optical properties of the B-KPro devices permit 20/20 visual acuity. The limiting factors precluding normal visual acuity include compromised human retinal or optic nerve function, obstructions within the ocular media,[24–26] or surgical complications including tilt or decentration of the B-KPro implant.[27] Furthermore, the predicted postoperative refraction may be inaccurate due to postoperative changes in axial length due to lower or higher intraocular pressures than on preoperative testing.

Future opportunities to improve image quality of the B-KPro are multifold. First, if a singlet design continues to be pursued, the posterior surface of the B-KPro optic could be machined to include a second refractive surface whose radius of curvature can be optimized to minimize the spherical aberration.[14] Second, B-KPro devices could be manufactured to accommodate more sophisticated lens shapes, for example, through injection molding, in which an aspheric design could be adopted akin to toric IOL lenses to reduce HOA.[28] Third, a new class of *flat* refractive elements enabled by local nanoscale phase engineering has recently emerged.[29] This technology, known as metalenses, enables broadband achromatic focusing that suffers minimal optical aberration in applications for microscopy and endoscopy.[30,31] In the advent of scalable production of metalenses,[32,33] one might replace the curved surfaces for refraction with planar metalenses where aberrations can be minimized. This has the advantage of shifting the lens-machining burden in B-KPro manufacturing to the scalable top-down nanofabrication approach where phase-modulating patterns are lithographically defined on a planar substrate. With these avenues of reducing HOAs in future B-KPro devices,[34] we hypothesize there may be an improvement in patients' perceived vision and also an increased tolerance for device postimplantation decentration and the subsequent image degradation.

In the grand scheme of long-term vision preservation in B-KPro patients, there are other important nonoptical challenges to overcome, such as glaucoma, retroprosthetic membrane formation, infection, and retinal detachment. Recent laboratory studies have revealed an inflammatory, intraocular pressure–independent pathway to glaucoma,[16,24,25,35–39] and clinical studies have shown systemic elevation of tumor necrosis factor alpha and its receptor II in the blood of KPro patients.[16] Collectively, laboratory and clinical data suggest that targeted immunomodulation may be an important therapeutic adjunct to prevent glaucoma after corneal surgery.[24,25,35] Because clinical studies may take years to conclude, engineering and optical innovations[17,21,27,41–47] can be implemented in the meanwhile to improve the overall performance and safety of B-KPro surgery. In this respect, the present study provides valuable information that can aid in improvement in the B-KPro optics.

Conclusions

It is well known that the B-KPro can provide excellent visual acuity in patients with otherwise healthy eyes and clear ocular media. Our theoretical and experimental characterization at the bench-top further supports this finding. Further improvements in patients' visual experience can be achieved beyond 20/20 vision by attending to HOA correction, primarily by implemented an aspheric lens profile with negative Q-value. This would require shifting of the manufacturing process from computer numerical control (CNC) lathing to PMMA injection molding.

Acknowledgments

The authors thank Edward Pei at Institute of Optics at University of Rochester for his expertise and contribution to this work, and Eli Peli and Rony Sayegh from Massachusetts Eye and Ear for manuscript feedback.

Supported by the Boston Keratoprosthesis Research Fund, Massachusetts Eye and Ear.PCH, ET, JC, CHD, and EIP are, or have been, full-time employees of the Massachusetts Eye and Ear, a nonprofit hospital that distributes the Boston Keratoprosthesis.

Disclosure: **P.-C. Hui,** None; **L.A. Pereira,** None; **R. Dore,** None; **S. Chen,** None; **E. Taniguchi,** None; **J. Chodosh,** None; **C.H. Dohlman,** None; **E.I. Paschalis,** None

References

1. Dohlman CH, Cruzat A, White M. The Boston keratoprosthesis 2014: a step in the evolution of artificial corneas. *Spektrum der Augenheilkunde*. 2014;28:226–233.
2. Zerbe BL, Belin MW, Ciolino JB, Group BTKS. Results from the multicenter Boston type 1 keratoprosthesis study. *Ophthalmology*. 2006;113:1779–1784.e1.
3. Pujari S, Siddique SS, Dohlman CH, Chodosh J. The Boston keratoprosthesis type II: the Massachusetts eye and ear infirmary experience. *Cornea*. 2011;30:1298–1303.
4. Klufas MA, Colby KA. The Boston keratoprosthesis. *Int Ophthalmol Clin*. 2010;50:161–175.
5. Ament JD, Spurr-Michaud SJ, Dohlman CH, Gipson IK. The Boston Keratoprosthesis: comparing corneal epithelial cell compatibility with titanium and PMMA. *Cornea*. 2009;28:808.
6. Cruzat A, Tauber A, Shukla A, Paschalis EI, Pineda R, Dohlman CH. Low-cost and readily available tissue carriers for the Boston keratoprosthesis: a review of possibilities. *J Ophthalmol*. 2013;2013:686587.
7. Dohlman CH, Harissi-Dagher M, Graney J. The Boston keratoprosthesis: a new threadless design. *Digit J Ophthalmol*. 2007;13.
8. Al Arfaj K. Boston keratoprosthesis–clinical outcomes with wider geographic use and expanding indications–a systematic review. *Saudi J Ophthalmol*. 2015;29:212–221.
9. Rudnisky CJ, Belin MW, Guo R, Ciolino JB; Boston Type 1 Keratoprosthesis Study Group. Visual acuity outcomes of the Boston keratoprosthesis type 1: multicenter study results. *Am J Ophthalmol*. 2016;162:89–98.e1.
10. Sokol A, Bertelsen TI, Teigland N. The optical function of keratoprostheses. *Acta Ophthalmol (Copenh)*. 1977;55:317–332.
11. Sayegh RR, Avena Diaz L, Vargas-Martin F, Webb RH, Dohlman CH, Peli E. Optical functional properties of the Boston Keratoprosthesis. *Invest Ophthalmol Vis Sci*. 2010;51:857–863.
12. Langenbucher A, Szentmáry N, Speck A, Seitz B, Eppig T. Calculation of power and field of view of keratoprostheses. *Ophthalmic Physiol Opt : J Brit Coll of Ophthal Opticians (Optometrists)*. 2013;33(4), 412–419.
13. International Organization for Standardization. Ophthalmic Implants Intraocular Lenses Part 2: optical Properties and Test Methods. Geneva, Switzerland: ISO. 1999. pp. 127 (ISO 11979-2).

14. Wyant JC, Creath K. Basic wavefront aberration theory for optical metrology. *Appl Opt Optical Eng*. 1992;11:28–39.
15. Bennett H, Porteus J. Relation between surface roughness and specular reflectance at normal incidence. *JOSA*. 1961;51:123–129.
16. Paschalis EI, Taniguchi EV, Chodosh J, et al. Blood levels of tumor necrosis factor alpha and its type 2 receptor are elevated in patients with Boston type I keratoprosthesis. *Curr Eye Res*. 2019;42:1–8.
17. Sayegh RR, Dohlman CH, Greenstein SH, Peli E. The Boston keratoprosthesis provides a wide depth of focus. *Ophthalmic Physiol Opt*. 2015;35:39–44.
18. Martínez CE, Applegate RA, Klyce SD, McDonald MB, Medina JP, Howland HC. Effect of pupillary dilation on corneal optical aberrations after photorefractive keratectomy. *Arch Ophthalmol*. 1998;116:1053–1062.
19. Cade F, Cruzat A, Paschalis EI, Santo LE, Pineda R. Analysis of four aberrometers for evaluating lower and higher order aberrations. *PLoS One*. 2013;8:e54990.
20. Stasi K, Pantanell S, Sabesan R, Yoon G, McCormick G, Aquavella J. Characterization of higher order aberrations in eyes with Dohlman/Boston Keratoprostheses and comparison with penetrating keratoplasty and normal eyes. *Invest Ophthalmol Vis Sci*. 2008;49:1038.
21. Abdelaziz M, Dohlman CH, Sayegh RR. Measuring forward light scatter by the Boston keratoprosthesis in various configurations. *Cornea*. 2017;36:732–735.
22. Giraldez MJ, Yebra-Pimentel E. Hydrogel contact lenses surface roughness and bacterial adhesion. *Ocular Diseases*. IntechOpen; 2012.
23. Pérez-Merino P, Martinez-Garcia MC, Mar-Sardana S, et al. Corneal light transmission and roughness after refractive surgery. *Optom Vis Sci*. 2010;87:E469–E474.
24. Dohlman CH, Cade F, Regatieri CV, et al. Chemical burns of the eye: the role of retinal injury and new therapeutic possibilities. *Cornea*. 2018;37:248–251.
25. Dohlman CH, Zhou C, Lei F, et al. Glaucoma after corneal trauma or surgery—a rapid, inflammatory, IOP-independent pathway. *Cornea*. 2019;38:1589–1594.
26. Crnej A, Paschalis EI, Salvador-Culla B, et al. Glaucoma progression and role of glaucoma surgery in patients with Boston keratoprosthesis. *Cornea*. 2014;33:349–354.
27. Helms RW, Zhao X, Sayegh RR. Keratoprosthesis decentration and tilt results in degradation in image quality. *Cornea*. 2018;37:772–777.
28. Wang L, Koch DD. Custom optimization of intraocular lens asphericity. *J Cataract Refract Surg*. 2007;33:1713–1720.
29. Khorasaninejad M, Chen WT, Devlin RC, Oh J, Zhu AY, Capasso F. Metalenses at visible wavelengths: diffraction-limited focusing and subwavelength resolution imaging. *Science*. 2016;352:1190–1194.
30. Pahlevaninezhad H, Khorasaninejad M, Huang Y-W, et al. Nano-optic endoscope for high-resolution optical coherence tomography in vivo. *Nat Photonics*. 2018;12:540–547.
31. Tseng ML, Hsiao HH, Chu CH, et al. Metalenses: advances and applications. *Adv Opt Mater*. 2018;6:1800554.
32. She A, Zhang S, Shian S, Clarke DR, Capasso F. Large area metalenses: design, characterization, and mass manufacturing. *Opt Express*. 2018;26:1573–1585.
33. Park J-S, Zhang S, She A, et al. All-glass, large metalens at visible wavelength using deep-ultraviolet projection lithography. *Nano Lett*. 2019;19:8673–8682.
34. Bakshi SK, Paschalis EI, Graney J, Chodosh J. Lucia and beyond: development of an affordable keratoprosthesis. *Cornea*. 2019;38:492–497.
35. Chen X, Lei F, Zhou C, et al. Glaucoma after ocular surgery or trauma: the role of infiltrating monocytes and their response to cytokine inhibitors. *Am J Pathol*. 2020;190:2056–2066.
36. Paschalis EI, Zhou C, Lei F, et al. Mechanisms of retinal damage after ocular alkali burns. *Am J Pathol*. 2017;187:1327–1342.
37. Paschalis EI, Lei F, Zhou C, et al. Permanent neuroglial remodeling of the retina following infiltration of CSF1R inhibition-resistant peripheral monocytes. *Proc Natl Acad Sci USA*. 2018;115:E11359–E11368.
38. Dohlman CH, Robert MC, Paschalis EI. Treatment of chemical burn to the eye: A changing picture. In *Foundations of Corneal Disease 2020* Springer, Cham.; 2020:109–119.
39. Paschalis EI, Lei F, Zhou C, et al. The role of microglia and peripheral monocytes in retinal damage after corneal chemical injury. *Am J Pathol*. 2018;188:1580–1596.
40. Dohlman CH, Harissi-Dagher M, Graney J. The Boston keratoprosthesis: a new threadless design. *Digital J Ophthalmol*. 2007;13:3.
41. Bakshi SK, Graney J, Paschalis EI, et al. Design and outcomes of a novel keratoprosthesis: addressing unmet needs in end-stage cicatricial corneal blindness. *Cornea*. 2020;39:484–490.

42. Shanbhag SS, Saeed HN, Paschalis EI, Chodosh J. Boston keratoprosthesis type 1 for limbal stem cell deficiency after severe chemical corneal injury: a systematic review. *Ocul Surf*. 2018;16:272–281.
43. Paschalis EI, Chodosh J, Spurr-Michaud S, et al. In vitro and in vivo assessment of titanium surface modification for coloring the backplate of the Boston keratoprosthesis. *Invest Ophthalmol Vis Sci*. 2013;54:3863–3873.
44. Gonzalez-Andrades M, Sharifi R, Islam M-M, et al. Improving the practicality and safety of artificial corneas: pre-assembly and gamma-rays sterilization of the Boston Keratoprosthesis. *Ocul Surf*. 2018;16:322–330.
45. Todani A, Ciolino JB, Ament JD, et al. Titanium back plate for a PMMA keratoprosthesis: clinical outcomes. *Graefes Arch Clin Exp Ophthalmol*. 2011;249:1515–1518.
46. Wang L, Jeong KJ, Chiang HH, et al. Hydroxyapatite for keratoprosthesis biointegration. *Invest Ophthalmol Vis Sci*. 2011;52:7392–7399.
47. Islam M-M, Sharifi R, Mamodaly S, et al. Effects of gamma radiation sterilization on the structural and biological properties of decellularized corneal xenografts. *Acta Biomater*. 2019;96:330–344.